Progress In Electromagnetics Research B, Vol. 48, 131–149, 2013

CONVEX MESHFREE SOLUTIONS FOR ARBITRARY WAVEGUIDE ANALYSIS IN ELECTROMAGNETIC PROBLEMS

Lifang Wang*

Lawrence Livermore National Laboratory, Livermore, CA 94550, USA

Abstract—This paper presents a convex meshfree framework for solving the scalar Helmholtz equation in the waveguide analysis of electromagnetic problems. The generalized meshfree approximation (GMF) method using inverse tangent basis functions and cubic spline weight functions is employed to construct the first-order convex approximation which exhibits a weak Kronecker-delta property at the waveguide boundary and allows a direct enforcement of homogenous Dirichlet boundary conditions for the transverse magnetic (TM) mode analyses. Four arbitrary waveguide examples are analyzed to demonstrate the accuracy of the presented formulation, and comparison is made with the analytical, finite element and meshfree solutions.

1. INTRODUCTION

Waveguides used for the transmission of electromagnetic signals are important devices in optic and electronic applicants such as the optical fiber, microwave elements and radar. The design of waveguides that are able to propagate electromagnetic waves with low dispersion and low attenuation over large distances is a critical issue for the development of telecommunication systems. One typical way to evaluate propagation characteristics of waveguides with arbitrarily shaped cross section is to use finite element method. Unfortunately, the finite element simulation of electromagnetic wave propagation governed by the Helmholtz equation presents a notorious pollution error [1], a numerical error related to the phase difference between the exact and finite element solutions, particularly for problems with high wave numbers. To minimize the pollution error and obtain an accurate

Received 21 December 2012, Accepted 17 January 2013, Scheduled 26 January 2013
* Corresponding author: Lifang Wang (wang22@llnl.gov).

solution in the finite element analysis of Helmholtz equation, the resolution of meshes should be adjusted to the wave number according to the "rule of thumb" [2]. Many non-standard finite element methods have been developed in the past two decades to reduce the pollution error including Galerkin/Least Squares (GLS) Method [3], Generalized Finite Element Method [4], and Discontinuous Galerkin Method [5]. Nevertheless, it remains a challenge to design accurate, robust and efficient numerical algorithms for the Helmholtz equation, especially when high wave numbers or high oscillatory solutions are involved [6].

On the other hand, several meshfree methods [7–9] have recently been proposed to solve the Helmholtz equation in waveguide problems. In comparison with the standard finite element method, the characteristics of mesh-independent and wave-based approximation effectively make the meshfree methods attractive alternative numerical techniques for modeling the waveguide problems. Conventional meshfree approximations such as Moving Least-Squares (MLS) approximation [10] and Reproducing Kernel (RK) approximation [11] do not satisfy the Kronecker-delta property at the boundary. Therefore, special treatments such as Lagrange multiplier are required to impose the essential boundary conditions. However, the method of Lagrange multiplier involves more unknowns and may result in an indefinite discrete linear system. Other meshfree interpolation methods based on radial basis functions (RBF) [12] were also developed for waveguide analysis [13–15]. Significant accuracy improvements have been made in particular for the high frequency modes. While such methods provide high fidelity predictions of the propagation properties in waveguides, the issues of high conditioning, irregular nodal distribution and boundary effect due to the characteristics of non-locality and over-determined system of equations in RBF methods have not yet been fully investigated.

Recently a novel approximation scheme, the generalized meshfree (GMF) approximation method [16], was developed to enhance the smoothness of the approximation as well as to generate the desired weak Kronecker-delta property [16] at the boundary. The meshfree convex approximation [16] generated by GMF approximation method was shown to be more robust than the non-convex meshfree approximation such as conventional MLS and RK approximations when the low-order Gaussian quadrature is used for the numerical integration. The meshfree convex approximation was also found to be insensitive to the nodal support size in solving the elastostatic problems. The purpose of this study is to present an analysis of waveguide problems using the meshfree convex approximation. This paper is divided into six sections. In Section 2 of this paper,

the scalar Helmholtz equation in waveguide problem is reviewed. The construction of meshfree convex approximation is described in Section 3. Section 4 gives the final discrete equations. Four numerical examples are studied in Section 5. Final conclusions are made in Section 6.

2. SCALAR HELMOLTZ EQUATION

In this study, the general form of Maxwell's equations for waveguide analysis considers a non-magnetic and linear medium in vacuum without charges and currents. The electromagnetic waves are described by the electric field strength $\mathbf{E}$, the electric flux density $\mathbf{D}$, the magnetic field strength $\mathbf{H}$, and the magnetic flux density $\mathbf{B}$ through the following time dependent first-order equations:

$$\nabla \times \mathbf{H} = \frac{\partial \mathbf{D}}{\partial t} \tag{1}$$

$$\nabla \times \mathbf{E} = -\frac{\partial \mathbf{B}}{\partial t} \tag{2}$$

$$\nabla \cdot \mathbf{D} = 0 \tag{3}$$

$$\nabla \cdot \mathbf{B} = 0. \tag{4}$$

The symbol $\nabla\times$ denotes the curl operator and $\nabla\cdot$ is the divergence operator. The relationships between electric flux density $\mathbf{D}$ and electric field $\mathbf{E}$ as well as magnetic flux density $\mathbf{B}$ and magnetic field $\mathbf{H}$ are defined by the following constitutive equations:

$$\mathbf{D} = \varepsilon \mathbf{E} \tag{5}$$

$$\mathbf{B} = \mu \mathbf{H}, \tag{6}$$

where ε and μ are permittivity and permeability, respectively and considered constants in time. By assuming the electromagnetic fields $\mathbf{E}$, $\mathbf{D}$, $\mathbf{H}$ and $\mathbf{B}$ to be time-harmonic, one can transform the time-dependent Maxwell equations to a second-order wave equation in frequency domain and can solve it numerically. This wave equation is known as the scalar Helmholtz equation and is expressed in two-dimensional case by

$$\nabla^2 \phi(\mathbf{x}) + k_c^2 \phi(\mathbf{x}) = 0, \quad \mathbf{x} \in \Omega \subset \Re^2, \tag{7}$$

where $k_c = \omega\sqrt{\mu\varepsilon} = 2\pi/\lambda_c$ is the cutoff wavenumber with ω denoting the angular frequency and λ_c being the cutoff wavelength. Ω is a simply or multiply connected domain with boundary $\partial\Omega$. The two-dimensional scalar Helmholtz equation considers the cross section of the medium that is infinitely extended in z-direction. Therefore, when the electric field is normal to the cross section, one has $\phi = E_z$ which

corresponds to the transverse magnetic (TM) waves. The TM waves satisfy the following homogenous Dirichlet boundary condition:

$$\phi = 0 \quad \text{on} \quad \partial\Omega. \tag{8}$$

Consequently, when $\phi = H_z$ it represents the transverse electric (TE) waves which satisfy the homogenous Neumann boundary condition

$$\partial_n \phi = 0 \quad \text{on} \quad \partial\Omega. \tag{9}$$

The weak solution corresponding to the strong form in (7) $\sim$ (9) can be obtained by finding $\phi \in H^1(\Omega)$ such that

$$a(\phi, w) = 0 \quad \forall \quad w \in H_0^1(\Omega), \tag{10}$$

where

$$a(\phi, w) = \int_\Omega \nabla\phi \cdot \nabla w d\Omega - \int_\Omega k_c^2 \phi w d\Omega \tag{11}$$

H^1 is the standard Sobolev space of order one and $H_0^1(\Omega) = \left\{ w \in H^1(\Omega), w|_{\partial\Omega} = 0 \right\}$.

3. CONVEX MESHFREE APPROXIMATION

In this section, a first-order generalized meshfree (GMF) convex approximation is employed to approximate the scalar function ϕ for waveguide analysis. The fundamental idea of the GMF approximation [16] is the introduction of an enriched basis function in the Shepard function to achieve linear consistency. The choice of the basis function determines whether the GMF approximation has convexity property. In this paper, a convex GMF approximation constructed using an inverse tangent basis function is employed in the approximation of electromagnetic wave equation. Assume a convex hull $C(P)$ of a node set $P = \{\mathbf{x}_i, i = 1, \ldots, n\} \subset \Re^2$ defined by [16]

$$C(P) \equiv \left\{ \sum_{i=1}^{n} \alpha_i \mathbf{x}_i \,\middle|\, \mathbf{x}_i \in P,\ \alpha_i \in \Re^+ \cup \{0\}, \sum_{i=1}^{n} \alpha_i = 1 \right\}. \tag{12}$$

The GMF method is to construct convex approximations of a given function ϕ in the form

$$\phi^h(\mathbf{x}) = \sum_{i=1}^{n} \varphi_i(\mathbf{x}) \phi_i \tag{13}$$

with the generating function $\varphi_i : C(P) \to \Re$ satisfying the following polynomial reproduction property

$$\sum_{i=1}^{n} \varphi_i(\mathbf{x}) \mathbf{x}_i = \mathbf{x} \quad \forall \quad \mathbf{x} \in C(P). \tag{14}$$

The first-order GMF approximation in two-dimensions is expressed as

$$\varphi_i(\mathbf{x},\lambda_r) = \frac{\kappa_i}{\kappa} = \frac{\psi_a(\mathbf{x};\mathbf{x}-\mathbf{x}_i)\,\mathbf{B}_i(\mathbf{x}-\mathbf{x}_i,\lambda_r)}{\sum_{j=1}^{n}\psi_a(\mathbf{x};\mathbf{x}-\mathbf{x}_j)\,\mathbf{B}_j(\mathbf{x}-\mathbf{x}_j,\lambda_r)}, \tag{15}$$

and is subjected to linear constraints

$$\mathbf{Z}_r(\mathbf{x},\lambda_r) = \sum_{i=1}^{n}\varphi_i\cdot(\mathbf{x}-\mathbf{x}_i) = 0, \tag{16}$$

where

$$\kappa_i = \psi_a(\mathbf{x};\mathbf{x}-\mathbf{x}_i)\,\mathbf{B}_i(\mathbf{x}-\mathbf{x}_i,\lambda_r), \tag{17}$$

$$\kappa = \sum_{i=1}^{n}\kappa_i = \sum_{i=1}^{n}\psi_a(\mathbf{x};\mathbf{x}-\mathbf{x}_i)\,\mathbf{B}_i(\mathbf{x}-\mathbf{x}_i,\lambda_r). \tag{18}$$

The notation $\psi_a(\mathbf{x};\mathbf{x}-\mathbf{x}_i)$ in (15) represents the weight function of node i with support size $supp(\psi_a(\mathbf{x};\mathbf{x}-\mathbf{x}_i)) = a_i$. $B_i(\mathbf{x}-\mathbf{x}_i,\lambda_r)$ denotes the basis function of the GMF approximation. $\mathbf{x}$ is the coordinate of the evaluation point and $\mathbf{x}_i = [x_i, y_i]^T$ is the coordinate of node i. The symbol n in summations denotes the number of nodes within the support size $a(\mathbf{x})$ at fixed $\mathbf{x}$. $\lambda_r(\mathbf{x})(r=2)$ are the constraint parameters which have to be determined. An example of 2D convex hull of a finite set is illustrated in Fig. 1 where the dashed square represents a support size of a node. A tensor product cubic spline function with a rectangular support size of a_i with respect to node i is chosen to be the weight function in (15) and is defined by

$$\psi_a(\mathbf{x};\mathbf{x}-\mathbf{x}_i) = \psi\left(\frac{x-x_i}{a_i}\right)\psi\left(\frac{y-y_i}{a_i}\right), \tag{19}$$

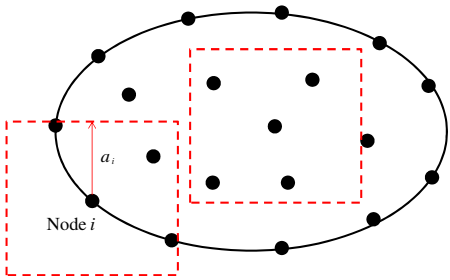

Figure 1. Convex hull of a finite node set in 2D where "a_i" denotes the support size of node "i".

where cubic spline function in one-dimensional space is given by

$$\psi(z_i) = \begin{cases} \dfrac{2 - 4z_i^2 + 4z_i^3}{3} & \text{for } 0 \le |z_i| \le \frac{1}{2} \\ \dfrac{4}{3} - 4z_i + 4z_i^2 - \dfrac{4}{3}z_i^3 & \text{for } \frac{1}{2} \le |z_i| \le 1 \\ 0 & \text{otherwise} \end{cases}. \tag{20}$$

In the GMF approximation, the property of the partition of unity is automatically satisfied by the normalization in (15). The completion of the GMF approximation is achieved by finding λ to satisfy (16). To determine λ at any fixed $\mathbf{x}$ in (15), a root-finding algorithm is required for the non-linear basis functions. In this study, the Newton-Raphson method is adopted for solving the objective function in (16). The partial derivative of the objective function with respect to λ is

$$\mathbf{J} = \sum_{i=1}^{n} \left[\left(\frac{\psi_a \mathbf{B}_{i,\lambda_r}}{\kappa} \right) \otimes (\mathbf{x} - \mathbf{x}_i) \right] - \mathbf{Z}_r \otimes \sum_{j=1}^{n} \left(\frac{\psi_a \mathbf{B}_{j,\lambda_r}}{\kappa} \right), \tag{21}$$

where $\mathbf{J}$ is a 2×2 Jacobian matrix, and $\otimes$ indicates the dyadic product of vectors. Once the converged λ is obtained, the basis functions are computed and the spatial derivative of the GMF approximation can be obtained and given by

$$\nabla \varphi_i = \varphi_{i,x} + \varphi_{i,\lambda_r} \lambda_{r,x}, \tag{22}$$

where

$$\varphi_{i,x} = \frac{\kappa_{i,x}}{\kappa} - \varphi_i \sum_{j=1}^{n} \frac{\kappa_{j,x}}{\kappa}, \tag{23}$$

$$\kappa_{i,x} = \psi_{a,x} \mathbf{B}_i + \psi_a \mathbf{B}_{i,x}, \tag{24}$$

$$\varphi_{i,\lambda_r} = \frac{\psi_a \mathbf{B}_{i,\lambda_r}}{\kappa} - \varphi_i \sum_{j=1}^{n} \left(\frac{\psi_a \mathbf{B}_{j,\lambda_r}}{\kappa} \right), \tag{25}$$

$$\mathbf{B}_i(\mathbf{x} - \mathbf{x}_i, \lambda_r) = 1 + \frac{2}{\pi} \tan^{-1}\left((x - x_i)\lambda_1 + (y - y_i)\lambda_2 \right), \tag{26}$$

$$\lambda_{r,x} = -\mathbf{J}^{-1} \mathbf{Z}_{r,x}, \tag{27}$$

$$\mathbf{Z}_{r,x} = \sum_{i=1}^{n} \varphi_{i,x} (\mathbf{x} - \mathbf{x}_i) + 1. \tag{28}$$

The resultant convex approximation poses a weak Kronecker-delta property at the boundary that allows a direct enforcement of homogenous essential boundary conditions in (8).

Figures 2(a) and (b) present two types of convex meshfree shape functions used in this study. For the nodes whose nodal supports do not

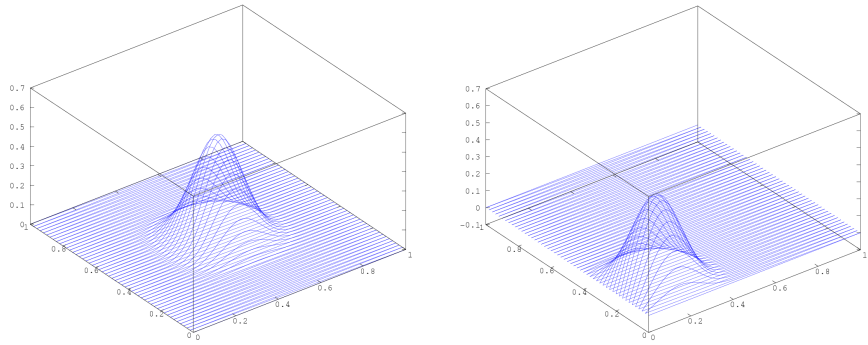

(a) (b)

Figure 2. Convex meshfree shape functions using an inverse tangent basis function. (a) Nodal support does not cover the global boundary. (b) Nodal support covers the global boundary.

intersect the global boundary, their shape functions are nonnegative as illustrated in Fig. 2(a). The rest of the nodes whose nodal supports intersect the global boundary, their shape functions remain nonnegative but decay to zero near the global boundary as shown in Fig. 2(b).

4. DISCRETE EQUATIONS

Standard Galerkin formulation is obtained by introducing the approximation of scalar function ϕ^h and test function w^h using (13) to the weak form in (10) to find convex meshfree solution $\phi^h \in H^1(\Omega)$ such that

$$a\left(\phi^h, w^h\right) = 0 \quad \forall \quad w^h \in H_0^1\left(\Omega\right). \tag{29}$$

The resulting system of linear equations is an eigenvalue problem and has the form

$$\mathbf{A}\boldsymbol{\varphi}^h = \left(\mathbf{K} - k_c^2\mathbf{M}\right)\boldsymbol{\varphi}^h = 0, \tag{30}$$

where $\boldsymbol{\varphi}^h = \{\phi_i\}^T$ is the vector of nodal solution. The components of stiffness matrix and mass matrix are given by

$$K_{ij} = \int_\Omega \mathbf{B}_i^T \mathbf{B}_j d\Omega \tag{31}$$

$$\mathbf{M}_{ij} = \int_\Omega \varphi_i \varphi_j d\Omega \tag{32}$$

$$\mathbf{B}_i = \begin{bmatrix} \frac{\partial \varphi_i}{\partial x} \\ \frac{\partial \varphi_i}{\partial y} \end{bmatrix}. \tag{33}$$

In this study, a finite element pre-processor is adopted to generate the discrete nodes for the meshfree computation. In addition, the generated finite elements are serviced as the integration cells and utilized for the numerical integration of (31) and (32). In order to evaluate the accuracy of the present method in the waveguide analysis, a 5-point Gauss quadrature rule is used in each integration cell. The eigenvalues and associated mode shapes in (30) are solved by the Lanczos method [17].

5. NUMERICAL EXAMPLES

Three examples are considered in this study to evaluate the performance of the presented method for the waveguide analysis in electromagnetic problems. A dimensionless unit system is used for simplicity. A normalized nodal support of 3.0 is considered for the construction of convex meshfree approximation as described in Section 3. As a comparison, the finite element solution using the standard bilinear quadrilateral elements and meshfree solution using radial basis function method [14] are provided.

5.1. Rectangular Waveguide

The first numerical example considers a rectangular waveguide with the dimension of 22.86×10.16 for the geometry shown in Fig. 3. In order to compare the solution in [14], same discretization using 31×14 uniformly distributed nodes are adopted for the convex meshfree analysis as well as for the finite element analysis. Table 1 compares the cutoff wavelengths and their relative errors for first ten TE modes

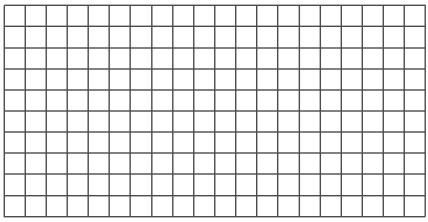

Figure 3. Discretization in rectangular waveguide problem.

Table 1. Cutoff wavelength and relative errors of TE mode for rectangular waveguide.

Mode	Analytical [18]	FEM (Err %)	r^5RBF (Err %) [14]	Present (Err %)
TE_1	4.5720	4.5699 (0.05)	4.5780 (0.13)	4.5720 (0.00)
TE_2	2.2860	2.2818 (0.18)	2.2918 (0.25)	2.2860 (0.00)
TE_{01}	2.0320	2.0271 (0.24)	2.0385 (0.32)	2.0320 (0.00)
TE_{11}	1.8569	1.8530 (0.21)	1.8549 (0.11)	1.8569 (0.00)
TE_{30}	1.5240	1.5178 (0.41)	1.5290 (0.33)	1.5240 (0.00)
TE_{21}	1.5187	1.5154 (0.21)	1.5097 (0.59)	1.5187 (0.00)
TE_{31}	1.2192	1.2149 (0.35)	1.2106 (0.71)	1.2192 (0.00)
TE_{40}	1.1430	1.1347 (0.73)	1.1485 (0.48)	1.1430 (0.00)
TE_{02}	1.0160	1.0062 (0.97)	1.0235 (0.74)	1.0160 (0.00)
TE_{41}	0.9962	0.9901 (0.61)	0.9921 (0.41)	0.9962 (0.00)

using three numerical methods. The relative error of cutoff wavelength is defined by

$$\text{Error} = \frac{\left|\lambda_c^a - \lambda_c^h\right|}{\lambda_c^a}, \tag{34}$$

where λ_c^h is the numerical cutoff wavelength defined in Section 2 and λ_c^a is the associated analytical cutoff wavelength. In Table 1, FEM and RBF methods produce same level of errors. On the other hand, the presented method produces an excellent result which is almost error-free for the first ten cutoff wavelengths in TE modes. Superior performance of the presented method over the other two methods is also demonstrated in the TM mode analysis. As in the TE mode analysis, the present method generates a very accurate solution in the TM mode analysis. Compares to the relative errors in TE mode, the relative errors in TM mode using RBF method have been greatly reduced.

5.2. Right-angle Triangular Waveguide

The second example considers the waveguide with a right-angle triangular cross-section. The right-angle triangle is a bisection of a square waveguide with the width equal to $\sqrt{2}$. The discretization of the waveguide shown in Fig. 4 is the same as the one used in [14] and is used for the finite element method and the presented method in this example.

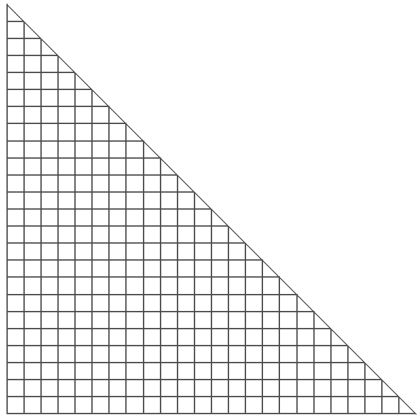

Figure 4. Discretization in right-angle triangular waveguide problem.

Table 2. Cutoff wavelength and relative errors of TM mode for rectangular waveguide.

Mode	Analytical [18]	FEM (Err %)	r^5RBF (Err %) [14]	Present (Err %)
TM_{11}	1.8569	1.8530 (0.21)	1.8570 (0.01)	1.8569 (0.00)
TM_{21}	1.5187	1.5155 (0.21)	1.5185 (0.01)	1.5187 (0.00)
TM_{31}	1.2192	1.2149 (0.35)	1.2187 (0.04)	1.2192 (0.00)
TM_{41}	0.9962	0.9901 (0.61)	0.9958 (0.04)	0.9962 (0.00)
TM_{12}	0..9918	0.9826 (0.92)	0.9929 (0.11)	0.9918 (0.00)
TM_{22}	0.9284	0.9206 (0.84)	0.9289 (0.05)	0.9284 (0.00)
TM_{32}	0.8454	0.8386 (0.80)	0.8452 (0.02)	0.8454 (0.00)
TM_{51}	0.8339	0.8257 (0.99)	0.8337 (0.02)	0.8339 (0.00)
TM_{42}	0.7594	0.7528 (0.87)	0.7587 (0.09)	0.7594 (0.00)
TM_{61}	0.7135	0.7031 (1.46)	0.7135 (0.00)	0.7135 (0.00)

Table 3 reports the comparison of cutoff wavelengths and corresponding relative errors of TE mode using three numerical methods. As shown in Table 3, the presented method outperforms the other two methods in terms of the relative errors. In comparison to finite element method, the RBF method effectively minimizes the relative errors of cutoff wavelength in TE mode in particular for the higher-order modes. However the errors in RBF method are still

Table 3. Cutoff wavelengths and relative errors of TE mode for right-angle triangular waveguide.

Mode	Analytical [14]	FEM (Err %)	r^{5}RBF (Err %) [14]	Present (Err %)
TE_1	2.8284	2.8264 (0.07)	2.8267 (0.06)	2.8284 (0.00)
TE_2	2.0000	1.9986 (0.07)	1.9941 (0.30)	2.0000 (0.00)
TE_3	1.4142	1.4102 (0.28)	1.4127 (0.11)	1.4142 (0.00)
TE_4	1.0000	0.9971 (0.30)	0.9945 (0.55)	1.0000 (0.00)
TE_5	0.9428	0.9368 (0.63)	0.7065 (0.09)	0.9428 (0.00)
TE_6	0.7071	0.6992 (1.12)	0.7065 (0.09)	0.7071 (0.00)
TE_7	0.6667	0.6622 (0.67)	0.6621 (0.69)	0.6667 (0.00)
TE_8	0.5657	0.5600 (1.03)	0.5662 (0.09)	0.5657 (0.00)

Table 4. Cutoff wavelengths and relative errors of TM mode for right-angle triangular waveguide.

Mode	Analytical [14]	FEM (Err %)	r^{5}RBF (Err %) [14]	Present (Err %)
TM_{11}	1.2649	1.2619 (0.24)	1.2649 (0.00)	1.2649 (0.00)
TM_{21}	0.7845	0.7803 (0.54)	0.7844 (0.01)	0.7845 (0.00)
TM_{12}	0.6860	0.6787 (1.07)	0.6864 (0.06)	0.6860 (0.00)
TM_{31}	0.5657	0.5603 (0.96)	0.5655 (0.04)	0.5657 (0.00)
TM_{22}	0.5252	0.5170 (1.56)	0.5255 (0.06)	0.5252 (0.00)
TM_{13}	0.4650	0.4536 (2.46)	0.4658 (0.17)	0.4650 (0.00)
TM_{41}	0.4417	0.4350 (1.51)	0.4477 (1.36)	0.4417 (0.00)
TM_{32}	0.4216	0.4126 (2.15)	0.4218 (0.05)	0.4216 (0.00)

noticeable. In contrast, a very accurate solution is obtained by the presented method in TM mode analysis as reported in Table 4.

Figures 5 and 6 show the comparison of relative errors in the first thirty-three cutoff wavenumbers using finite element method and the presented method for TE mode and TM mode respectively. The unbounded errors in finite element solution indicate the pollution effect of polynomial type numerical methods. In other words, the quality of the finite element solution depends significantly on the wavenumber k_c. The results in Figs. 5 and 6 also imply that the presented method can effectively minimize the pollution error and accurately reproduce the oscillatory solution for higher wavenumbers under the same finite

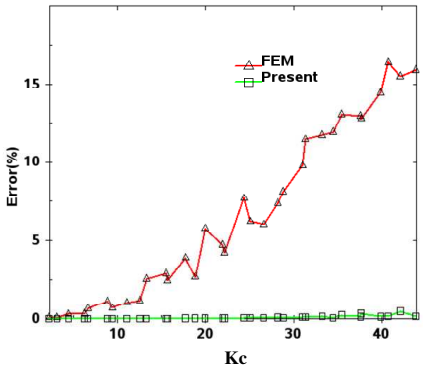

Figure 5. Comparison of relative errors in cutoff wavenumbers for thirty-three lowest-order TE modes.

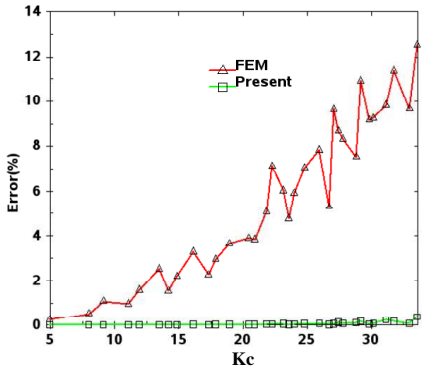

Figure 6. Comparison of relative errors in cutoff wavenumbers for thirty-three lowest-order TM modes.

element discretization. Four TM modes using the presented method are chosen and plotted in Fig. 7. All four TM mode fields predict the analytical mode fields accurately.

5.3. Circular Waveguide

Different from the regular discretization used in previous examples, this example studies the sensitivity of mesh irregularity to the solution of the proposed method. The cutoff wavenumbers for a circular waveguide of unit radius are studied in this example. A relative coarse discretization containing 209 nodes as depicted in Fig. 8 is used for the finite element analysis. Same discretization is adopted for the presented method. Tables 5 and 6 compare the cutoff wavenumbers and the corresponding relative errors for TE and TM modes respectively. The increasing relative errors of wavenumbers in shortwave modes predicted by finite element method indicate the pollution errors caused by the low density of finite element mesh which violates the "rule of thumb" On the contrary, the relative errors are well controlled under 0.5% using the presented method with same finite element discretization. The bounded relative errors generated by the presented method clearly are associated with the discretization errors and not the pollution errors. This result is consistent with the observations in two previous examples. Six computed TE and TM modes using the presented method are selected and plotted in Fig. 9 Fields for all six modes are in good agreement with the fields from the analytical solutions.

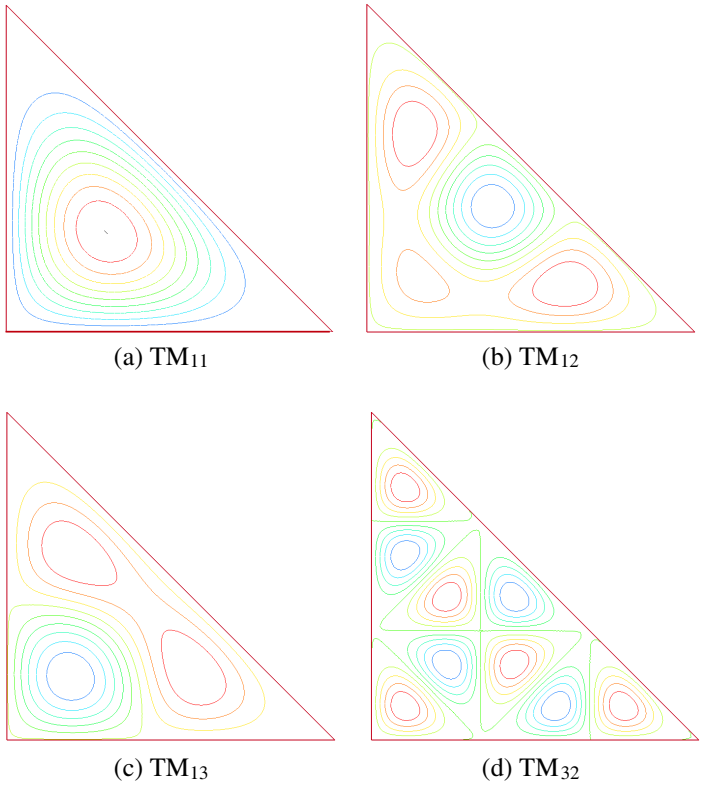

Figure 7. Field distribution of TM modes for right-angular triangular waveguide.

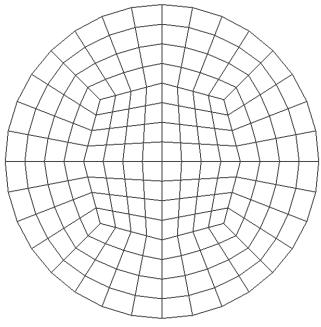

Figure 8. Discretization in circular waveguide problem.

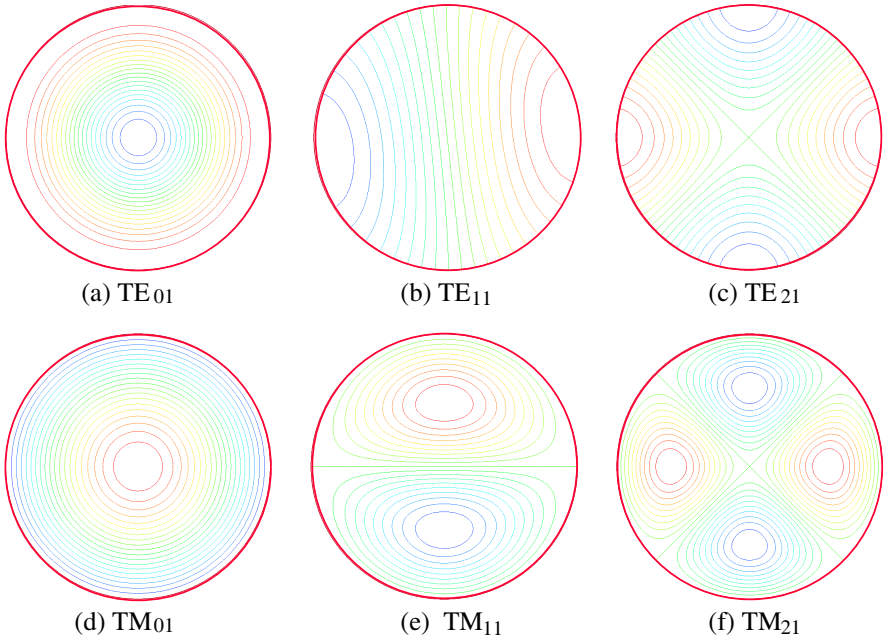

Figure 9. Field distribution of TE and TM modes for circular waveguide.

Table 5. Cutoff wave numbers and relative errors of TE modes for circular waveguide.

Mode	Analytical [19]	FEM (Err %)	Present (Err %)
TE_{11}	1.8412	1.8497 (0.46)	1.8472 (0.33)
TE_{21}	3.0542	3.0767(0.74)	3.0654 (0.33)
TE_{01}	3.8317	3.8792 (1.24)	3.8450 (0.35)
TE_{02}	5.3314	5.4225 (1.71)	5.3513 (0.37)
TE_{22}	6.7061	6.8455 (2.08)	6.7322 (0.39)
TE_{03}	7.0156	7.2328 (3.10)	7.0454 (0.42)
TE_{13}	8.5363	8.9099 (4.38)	8.5767 (0.47)
TE_{23}	9.9695	10.4341 (4.66)	9.9208 (0.49)

Table 6. Cutoff wave numbers and relative errors of TM modes for circular waveguide.

Mode	Analytical [19]	FEM (Err %)	Present (Err %)
TM_{01}	2.4048	2.4191 (0.60)	2.4136 (0.37)
TM_{11}	3.8317	3.8662 (0.90)	3.8456 (0.36)
TM_{21}	5.1356	5.2025 (1.30)	5.1549 (0.38)
TM_{02}	5.5201	5.6330 (2.05)	5.5403 (0.37)
TM_{12}	7.0156	7.2145 (2.84)	7.0414 (0.37)
TM_{22}	8.4172	8.6724 (3.03)	8.4489 (0.38)
TM_{03}	8.6537	9.0154 (4.18)	8.6864 (0.38)
TM_{13}	10.1735	10.7559 (5.73)	10.2127(0.39)
TM_{23}	11.6198	12.3496 (6.28)	11.6644 (0.38)

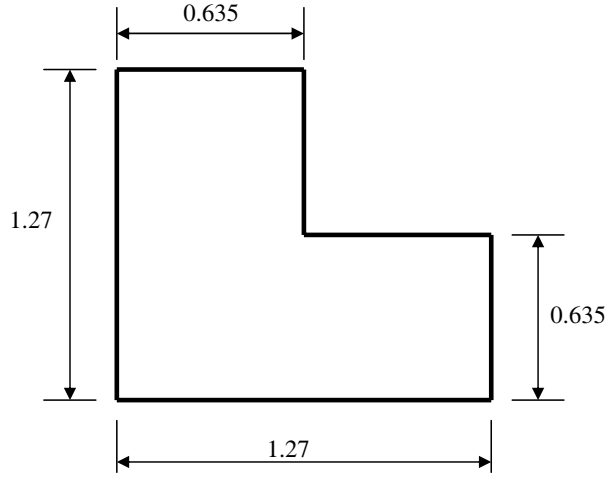

Figure 10. Problem domain for L-shape waveguide.

5.4. L-shaped Waveguide

This example presents an analysis of the waveguide containing boundary singularities such as a reentrant corner in a L-shaped waveguide. The geometry of the L-shaped waveguide is shown in Fig. 10. The mesh used for the finite element analysis is given in Fig. 11(a) which contains 234 nodes. Same discretization is also used for the proposed method. Since the analytical solution for this problem is not available, a reference solution is obtained by the

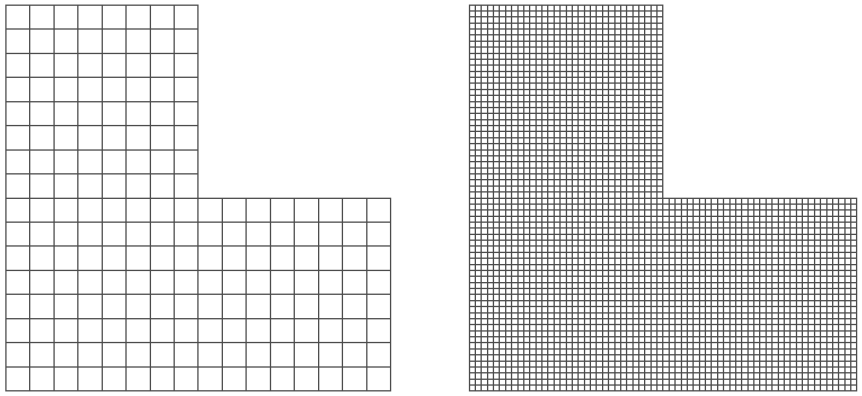

(a) Mesh used for comparison (b) Mesh used for reference solution

Figure 11. Discretization in L-shaped waveguide problem.

Table 7. Cutoff wavenumbers and relative errors of TE mode for L-shaped waveguide.

Mode	Reference	FEM (Err %)	Present (Err %)
TE_1	1.9142	1.9220 (0.41)	1.9206 (0.33)
TE_2	2.9608	2.9658 (0.17)	2.9608 (0.00)
TE_3	4.9494	4.9792 (0.60)	4.9487 (0.01)
TE_4	4.9494	4.9792 (0.60)	4.9487 (0.01)
TE_5	5.3166	5.3449 (0.53)	5.3155 (0.02)
TE_6	5.5871	5.6240 (1.86)	5.5932 (0.11)
TE_7	6.9995	7.0417 (0.60)	6.9995 (0.00)
TE_8	7.2974	7.4000 (1.41)	7.3089 (0.16)
TE_9	7.6156	7.7171 (1.33)	7.6112 (0.06)
TE_{10}	8.4136	8.5128 (1.18)	8.4256 (0.14)

finite element method using a refined mesh as shown in Fig. 11(b). On the other hand, the computational domain of such problem is non-convex. Therefore, special treatments such as the parametric approach [20] for approximating the non-convex domain is required for the meshfree analysis using convex approximation. Another simple approach which is used in this study to maintain the convexity in meshfree approximation and therefore avoids any special treatments is to properly adjust the nodal supports of the nodes near the reentrant

Table 8. Cutoff wavenumbers and relative errors of TM mode for L-shaped waveguide.

Mode	Reference	FEM (Err %)	Present (Err %)
TM_1	4.8934	4.9275 (0.70)	4.8807 (0.26)
TM_2	6.1416	6.1784 (0.60)	6.1446 (0.05)
TM_3	6.9995	7.0417 (0.60)	7.0044 (0.07)
TM_4	8.5630	8.6608 (1.14)	8.5718 (0.10)
TM_5	8.9074	9.0400 (1.49)	8.9028 (0.05)
TM_6	10.1579	10.3803 (2.19)	10.1669 (0.09)
TM_7	10.5739	10.8125 (2.26)	10.6001(0.25)
TM_8	11.0778	11.3061 (2.06)	11.0954 (0.16)
TM_9	11.0778	11.3061 (2.06)	11.0954 (0.16)
TM_1	11.8766	12.1191 (2.04)	11.8901 (0.11)

corner. The principle for the selection of the nodal supports is that the line segment between a node and its supporting node should not be outside the computation domain Ω.

The comparison of relative errors is given in Table 7 and Table 8 for TE mode and TM mode respectively. While FEM produces errors increasing with cutoff wavenumbers, the proposed method presents errors which remain under control. For the first ten TE and TM modes, the relative errors of the proposed method are much smaller than those of FEM.

6. CONCLUSION

This paper presents a meshfree analysis of electromagnetic waveguides using the convex approximation. Four numerical examples are utilized to evaluate the performance of the presented method in the arbitrary waveguide analyses. The numerical results in this study suggest that the presented method can produce more accurate solution than the one obtained from the bilinear finite element method under the same discretization. In all four examples, the pollution errors in bilinear finite element solutions grow unbounded with the increase of the wavenumber. In contrast, the pollution errors in the presented method are effectively eliminated.

Since the presented method directly uses the finite element mesh for computation, it can be easily incorporated into the existing finite element code for the waveguide analysis. Compare to the other existing

meshfree methods for waveguide study, the presented method employs the convex approximation, and thus simplifies the boundary condition enforcements in the TE and TM modes analyses. The extension of presented method to the analysis of waveguide with non-convex cross-section such as coaxial line problems requires a revision of the current formulation. This will be presented in a forthcoming paper.

ACKNOWLEDGMENT

This work performed under the auspices of the U.S. Department of Energy by Lawrence Livermore National Laboratory under Contract DE-AC52-07NA27344.

REFERENCES

1. Ihlenburg, F. and I. Babuska, "Finite element solution of the Helmholtz equation with high wave number Part I: The h-version of FEM," *Comp. Math. Appl.*, Vol. 30, No. 9, 9–37, 1995.
2. Harari, I. and T. J. R. Hughes, "Finite element method for the Helmholtz equation in an exterior domain: Model problems," *Comp. Meth. Appl. Mech. Eng.*, Vol. 87, 59–96, 1991.
3. Harari, I. and T. J. R. Hughes, "Galerkin/least squares finite element method for the reduced wave equation with non-reflecting boundary conditions," *Comp. Meth. Appl. Mech. Eng.*, Vol. 92, 441–454, 1992.
4. Babuska, I., F. Ihlenburg, E. Paik, and S. Sauter, "A generalized finite element method for solving the Helmholtz equation in two dimensions with minimal pollution," *Comp. Meth. Appl. Mech. Eng.*, Vol. 128, 325–359, 1995.
5. Farhat, C., I. Harari, and L. P. Franca, "The discontinuous enrichment method," *Comp. Meth. Appl. Mech. Eng.*, Vol. 190, 6455–6479, 2001.
6. Zienkiewicz, O. C., "Achievements and some unsolved problems of the finite element method," *Int. J. Numer. Meth. Engrg.*, Vol. 47, 9–28, 2000.
7. Ooi, B. L. and G. Zhao, "Element-free method for the analysis of partially-filled dielectric waveguides," *Journal of Electromagnetic Waves and Applications*, Vol. 21, No. 2, 189–198, 2007.
8. Miao, Y., Y. Wang, and H. Wang, "A meshless hybrid boundary-node method for Helmholtz problems," *Eng. Anal. Boundary Elem.*, Vol. 33, 120–127, 2009.

9. Correa, B. C., E. J. Silva, A. R. Fonseca, D. B. Oliveria, and R. C. Mesquita, "Meshless local Petrov-Galerkin in solving microwave guide problems," *IEEE Trans. Magnetics*, Vol. 47, 1526–1529, 2011.
10. Belytschko, T., Y. Y. Lu, and L. Gu, "Element-free Galerkin methods," *Int. J. Numer. Meth. Engrg.* Vol. 37, 229–256, 1994.
11. Liu, W. K., S. Jun, and Y. F. Zhang, "Reproducing kernel particle methods," *Int. J. Numer. Meth. Fluids*, Vol. 20, 1081–1106, 1995.
12. Kansa, E. J., "Multiqudrics — A scattered data approximation scheme with applications to computational fluid-dynamics — I: Surface approximations and partial derivatives," *Comp. Math. Appl.*, Vol. 9, 127–145, 1992.
13. Jiang, P. L., S. Q. Li, and C. H. Chan, "Analysis of elliptic waveguides by a meshless collocation method with the Wendland radial basis functions," *Microwave and Optical Technology Letters*, Vol. 32, No. 2, 162–165, 2002.
14. Lai, S. J., B. Z. Wang, and Y. Duan, "Solving Helmholtz equation by meshless radial basis functions method," *Progress In Electromagnetics Research B*, Vol. 24, 351–367, 2010.
15. Kaufmann, T., Y. Yu, C. Engstrom, Z. Chen, and C. Fumeaux, "Recent developments of meshless radial point interpolation method for time-domain electromagnetics," *Int. J. Numer. Model: Elect. Networks, Devices and Fields*, Vol. 25, 468–489, 2012.
16. Wu, C. T., C. K. Park, and J. S. Chen, "A generalized meshfree approximation for the meshfree analysis of solids," *Int. J. Numer. Meth. Engrg.*, Vol. 85, 693–722, 2011.
17. Press, W. H., S. A. Teukolsky, W. T. Vetterling, and B. P. Flannery, *Numerical Recipes in Fortran 90*, 2nd Edition, Cambridge University Press, New York, 1996.
18. Harrington, R. F., *Time-harmonic Electromagnetic Fields*, Wiley-IEEE Press, New York, 2001.
19. Marcuvitz, N., *Waveguide Handbook*, Peter Peregrinus Ltd., London, 1993.
20. Shaw, A. and D. Roy, "NURBS-based parametric mesh-free methods," *Comput. Methods Appl. Mech. Engrg.*, Vol. 197, 1541–1567, 2008.